Surface-enhanced Raman scattering of graphene with photo-assisted-synthesized gold nanoparticles

Cheng-En Cheng,[1,2] Chi-Yuan Lin,[1,2] Hao-Yu Chang,[2,3] Chen-Han Huang,[4] Hsing-Ying Lin,[4] Chia-Hao Chen,[5] Chia-Chen Hsu,[3] Chen-Shiung Chang,[1] and Forest Shih-Sen Chien[2,6,*]

[1]*Department of Photonics and Institute of Electro-Optical Engineering, National Chiao Tung University, Hsinchu 30010, Taiwan*
[2]*Department of Physics, Tunghai University, Taichung 40704, Taiwan*
[3]*Department of Physics, National Chung Cheng University, Chiayi 62102, Taiwan*
[4]*Center for Nano Bio-Detection, National Chung Cheng University, Chiayi 62102, Taiwan*
[5]*National Synchrotron Radiation Research Center, Hsinchu 30076, Taiwan*
[6] *Tunghai Green Energy Development and Management Institute, Tunghai University, Taichung 40704, Taiwan*
** fsschien@thu.edu.tw*

Abstract: This paper presents a convenient and reliable method to prepare gold nanoparticles (AuNPs) on graphene. Photo-assisted synthesis (PAS) was employed to grow AuNPs in $AuCl_4^-$ electrolyte on graphene. The size of AuNPs could be as large as 130 nm. This optical method had a steady growth rate of AuNPs. The distribution of AuNPs was well controlled by focusing the laser for PAS. The minimum diameter of the distribution was approximately 1 μm. Surface-enhanced Raman scattering of graphene due to AuNPs was observed. Electrical fields near AuNPs calculated by the finite-difference time-domain algorithm ensured that the Raman enhancement was attributed to the localized surface plasmons of AuNPs.

OCIS codes: (240.6695) Surface-enhanced Raman scattering; (160.4236) Nanomaterials; (140.3450) Laser-induced chemistry.

References and links

1. E. Hutter and J. H. Fendler, "Exploitation of localized surface plasmon resonance," Adv. Mater. (Deerfield Beach Fla.) **16**(19), 1685–1706 (2004).
2. L. Authier, C. Grossiord, P. Brossier, and B. Limoges, "Gold nanoparticle-based quantitative electrochemical detection of amplified human cytomegalovirus DNA using disposable microband electrodes," Anal. Chem. **73**(18), 4450–4456 (2001).
3. A. J. Haes and R. P. Van Duyne, "A nanoscale optical biosensor: sensitivity and selectivity of an approach based on the localized surface plasmon resonance spectroscopy of triangular silver nanoparticles," J. Am. Chem. Soc. **124**(35), 10596–10604 (2002).
4. Y. Zhang, S. Liu, L. Wang, X. Qin, J. Tian, W. Lu, G. Chang, and X. Sun, "One-pot green synthesis of Ag nanoparticles-graphene nanocomposites and their applications in SERS, H_2O_2, and glucose sensing," RCS Adv. **2**(2), 538–545 (2012).
5. Y. Shao, J. Wang, H. Wu, J. Liu, I. A. Aksay, and Y. Lin, "Graphene based electrochemical sensors and biosensors: a review," Electroanalysis **22**(10), 1027–1036 (2010).
6. M. Pumera, A. Ambrosi, A. Bonanni, E. L. K. Chng, and H. L. Poh, "Graphene for electrochemical sensing and biosensing," Trends Analyt. Chem. **29**(9), 954–965 (2010).
7. W. Hong, H. Bai, Y. Xu, Z. Yao, Z. Gu, and G. Shi, "Preparation of gold nanoparticle/graphene composites with controlled weight contents and their application in biosensors," J. Phys. Chem. C **114**(4), 1822–1826 (2010).
8. M. Wirtz and C. R. Martin, "Template-fabricated gold nanowires and nanotubes," Adv. Mater. (Deerfield Beach Fla.) **15**(5), 455–458 (2003).
9. K. R. Brown, D. G. Walter, and M. J. Natan, "Seeding of colloidal Au nanoparticle solutions. 2. improved control of particle size and shape," Chem. Mater. **12**(2), 306–313 (2000).
10. Y. Shi, K. K. Kim, A. Reina, M. Hofmann, L.-J. Li, and J. Kong, "Work function engineering of graphene electrode via chemical doping," ACS Nano **4**(5), 2689–2694 (2010).

#180639 - $15.00 USD Received 27 Nov 2012; revised 16 Feb 2013; accepted 17 Feb 2013; published 8 Mar 2013

11. K. K. Kim, A. Reina, Y. Shi, H. Park, L.-J. Li, Y. H. Lee, and J. Kong, "Enhancing the conductivity of transparent graphene films via doping," Nanotechnology **21**(28), 285205 (2010).
12. J. Zhu, Y. Shen, A. Xie, L. Qin, Q. Zhang, and S. Zhang, "Photoinduced synthesis of anisotropic gold nanoparticles in room-temperature ionic liquid," J. Phys. Chem. C **111**(21), 7629–7633 (2007).
13. R. Klauser, I.-H. Hong, T.-H. Lee, G.-C. Yin, D.-H. Wei, K.-L. Tsang, T. J. Chuang, S.-C. Wang, S. Gwo, M. Zharnikov, and J.-D. Liao, "Zone-plate-based scanning photoelectron microscopy at SRRC: performance and applications," Surf. Rev. Lett. **09**(01), 213–222 (2002).
14. A. Taflove and S. C. Hagness, *Computational Electrodynamics: The Finite-Difference Time-Domain Method* (Artech House, Norwood, 2000).
15. P. B. Johnson and R. W. Christy, "Optical constants of the noble metals," Phys. Rev. B **6**(12), 4370–4379 (1972).
16. D. Lau and S. Furman, "Fabrication of nanoparticle micro-arrays patterned using direct write laser photoreduction," Appl. Surf. Sci. **255**(5), 2159–2161 (2008).
17. J.-W. Chen, C.-L. Wang, H. W. Shiu, C.-Y. Lin, C.-S. Chang, F. S.-S. Chien, C.-H. Chen, Y.-C. Chen, and C.-L. Wu, "Graphene on Au-coated SiO_x substrate: its core-level photoelectron microspectroscopy study," Appl. Phys. Express **5**(8), 085101 (2012).
18. N. R. Jana, L. Gearheart, and C. J. Murphy, "Evidence for seed-mediated nucleation in the chemical reduction of gold salts to gold nanoparticles," Chem. Mater. **13**(7), 2313–2322 (2001).
19. M. Moskovits, "Surface-enhanced Raman spectroscopy: a brief retrospective," J. Raman Spectrosc. **36**(6–7), 485–496 (2005).
20. O. Frank, G. Tsoukleri, I. Riaz, K. Papagelis, J. Parthenios, A. C. Ferrari, A. K. Geim, K. S. Novoselov, and C. Galiotis, "Development of a universal stress sensor for graphene and carbon fibres," Nat. Commun. **2**, 255 (2011).
21. T.-T. Liu, Y.-H. Lin, C.-S. Hung, T.-J. Liu, Y. Chen, Y.-C. Huang, T.-H. Tsai, H.-H. Wang, D.-W. Wang, J.-K. Wang, Y.-L. Wang, and C.-H. Lin, "A high speed detection platform based on surface-enhanced Raman scattering for monitoring antibiotic-induced chemical changes in bacteria cell wall," PLoS ONE **4**(5), e5470 (2009).
22. Z. Liu, C. Hu, S. Li, W. Zhang, and Z. Guo, "Rapid intracellular growth of gold nanostructures assisted by functionalized graphene oxide and its application for surface-enhanced Raman spectroscopy," Anal. Chem. **84**(23), 10338–10344 (2012).
23. L. Wu, H. S. Chu, W. S. Koh, and E. P. Li, "Highly sensitive graphene biosensors based on surface plasmon resonance," Opt. Express **18**(14), 14395–14400 (2010).

1. Introduction

Surface-enhanced Raman scattering (SERS), activated by localized surface plasmons (LSPs) of plasmonic nanostructures [1], have been widely used to enhance the sensitivity of electrochemical sensing or biosensing [2,3]. SERS has recently been applied to push the sensitivity of graphene-based sensing by an enhancement of 10^3 times [4]; graphene has been considered a promising base material for electrochemical sensing and biosensing [5,6]. Hong *et al.* presented a method to self-assembled gold nanoparticles (AuNPs) on functionalized graphene for biosensing [7]. However, to place AuNPs on graphene without chemical functionalization is difficult because the perfect lattice of graphene has no dangling bonds to cause chemical adsorption of AuNPs.

Chloroauric acid ($HAuCl_4$) aqueous solution is used for electroless Au plating [8] and AuNP synthesis [9]. In addition, electroless plating was employed to grow Au layer/nanostructures on chemical-vapor-deposited graphene [10,11]. One emerging approach for producing AuNPs with $AuCl_4^-$ solutions is by photochemical photo-assisted synthesis (PAS) [12], where AuNPs are synthesized in the $AuCl_4^-$ solution through UV light irradiation. In this article, we report the deposition of AuNPs with various sizes (under 130 nm in diameter) on pristine graphene at specific locations by PAS in $AuCl_4^-$ solution. PAS is an easy and reliable method, which requires only the $AuCl_4^-$ solution and has a steady volume growth rate of AuNPs. By atomic force microscopy (AFM), AuNPs were revealed to be produced by PAS but not electroless plating. In addition to synthesized AuNPs, a 2 nm thick Au layer was deposited on graphene by electroless plating simultaneously. The chemical composition of the plated Au thin layer was characterized by X-ray photoelectron spectroscopy (PES). The Raman signals of graphene with synthesized AuNPs were observed both *in situ* and *ex situ*. The Raman enhancement of graphene with a single 100 nm AuNP was as high as 10^3 times. From the calculation of the plasmonic electromagnetic (EM) field by the three-dimensional

#180639 - $15.00 USD Received 27 Nov 2012; revised 16 Feb 2013; accepted 17 Feb 2013; published 8 Mar 2013

(3D) finite-difference time-domain (FDTD) algorithm, the Raman enhancement was confirmed to be attributed to the LSP at the AuNPs.

2. Experimental and simulation modeling details

The graphene samples were prepared by mechanical exfoliation on the SiO_2/Si substrates to make the graphene visible under an optical microscope. The number of graphene layers was less than three layers, verified by Raman spectroscopy. The graphene samples were placed in a Petri dish, which was filled with deionized water. $AuCl_4^-$ solution was injected into the Petri dish to make an electrolyte of 4.3 mM concentration. The schematic of the experimental setup to prepare the AuNPs on gaphene by PAS and perform *in situ* Raman spectroscopy is shown in Fig. 1. The morphology of Au on the graphene sheet was characterized by scanning electron microscopy (SEM) and tapping-mode AFM (Agilent 5500 AFM). The chemical structures of graphene and Au were characterized with micro-PES (μ-PES) taken by scanning photoelectron microscopy (SPEM). Details of the SPEM system are described in Ref. 13. The Raman spectra of graphene were taken by a confocal optical system with a 633 nm He-Ne laser, the laser power to expose the sample was 3 mW and the spot size was 500 nm in diameter. The operating principle of the 3D FDTD algorithm to calculate the induced EM field of PAS of AuNP was based on the resolution of the discrete Curl-Maxwell's equations by iteration over time [[14]]. The Drude-Lorentz dispersion model and dielectric function measured by Johnson and Christy were employed in this calculation [15].

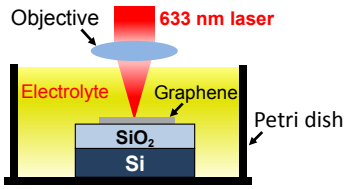

Fig. 1. Schematic of photo-assisted synthesis of AuNPs on graphene in $AuCl_4^-$ electrolyte and *in situ* micro Raman measurement (not to scale).

3. Results and discussion

Figure 2(a) shows the SEM images of synthesized AuNPs distributed on the graphene sheet and the inset displays a single AuNP obtained with a growth time (t) of 20 min. It is interesting to observe that no AuNP was produced on the bare SiO_2 surface during PAS. The dependence of the diameter $D(t)$ of AuNPs with t (i.e., the duration of laser irradiation to $AuCl_4^-$ solution) is shown in Fig. 2(b). AuNPs grew as large as 130 nm in diameter. The standard deviation of the diameter ranged between 10% and 25%. The increase of the diameter of AuNPs was well fitted by a cube root function of growth time,

$$D(t) = \sqrt[3]{\frac{6}{\pi}\alpha(t - t_0)}, \quad (1)$$

where the onset time of the nucleation of the AuNPs (t_0) = 1.8 min and the volume growth rate (α) = 2.35 × 10^4 nm^3/min were obtained. Thus, the volume of the AuNPs increased linearly with t. The AuNPs were suggested to be produced on graphene by PAS, where the laser light supplied the energy to facilitate the reduction of Au ions to AuNPs [11,12] by

$$2AuCl_4^- \xrightarrow{h\nu} 2Au^0 \downarrow + 3Cl_2 + 2Cl^-. \quad (2)$$

The volume growth rate was constant, so PAS of AuNPs was a reaction-limited process.

#180639 - $15.00 USD Received 27 Nov 2012; revised 16 Feb 2013; accepted 17 Feb 2013; published 8 Mar 2013

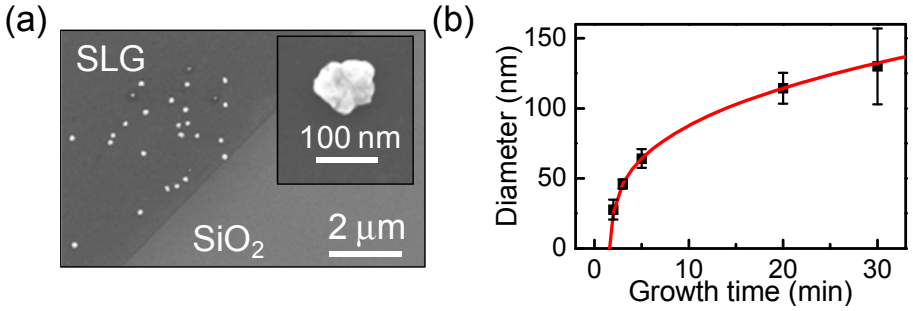

Fig. 2. (a) SEM images of synthesized AuNPs distributed on graphene. The inset is the image of a 100 nm Au NP on graphene after 20 min of PAS. (b) Growth of synthesized AuNPs with the time of PAS. The red curve shows the fitting with Eq. (1).

Typically, AuNPs are synthesized and deposited separately in chemical methods [7]. By PAS, synthesis and deposition of AuNPs on graphene were achieved by only one process with a single chemical ($AuCl_4^-$ electrolyte). Therefore, PAS is a convenient, efficient and reliable method of producing AuNPs with a diameter under 130 nm [predictable by Eq. (1)] with good uniformity. Compared with other physical methods for preparation of AuNPs (e.g., thermal evaporation and post-annealing), PAS is a low thermal-budget and less aggressive method, which is critical for many applications in biosensing. Moreover, PAS is activated by a laser light, so it is possible to pattern AuNPs on graphene, similar to laser direct writing [16]. The photochemical PAS can be controlled by the vector scanning of laser to achieve the patterning. The resolution of PAS patterning is related with the size of laser spots. Figure 3(a) shows the distribution of AuNPs varied with focusing of laser. As the laser spot was "in focus", two AuNPs were deposited within the area of a diameter < 1 μm, which is close to the diffraction limit. AuNPs scattered wider, if the laser was out of focus. The further the "out of focus" was, the wider the AuNPs scattered. Figure 3(b) shows the Raman mapping of G band over the area of "out of focus." The SERS of graphene due to LSP of AuNPs was observed. The SERS will be discussed later. Therefore, the distribution of AuNPs could be controlled by focusing the laser and the best resolution was about 1 μm. Note that the heat of laser power might cause the local disturbance of electrolyte, which had AuNPs distribute wider. Such a resolution is sufficient for many applications of biosensing. In addition, no photoresist has to be applied during PAS. The residues of photoresist on graphene are a contamination for the applications of graphene in biosensing and electronics.

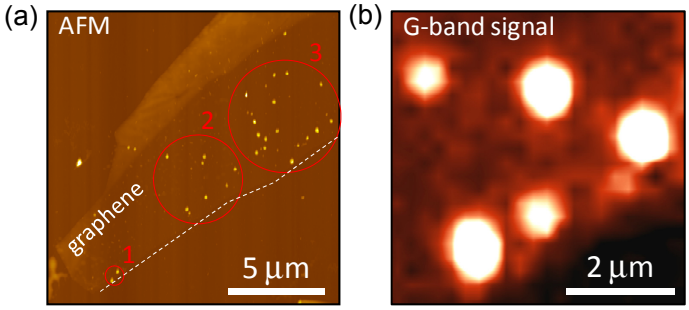

Fig. 3. (a) AFM image of AuNPs on graphene produced by different focusing of laser. The circles mark the areas of AuNPs under "in focus" (1), "out of focus" (2), and "further out of focus" (3) after 3 min irradiation each. The dashed line indicates the edge of graphene. (b) Raman mapping of G band (1560 cm^{-1} to 1620 cm^{-1}) taken over the area of "out of focus".

To verify that the mechanism for producing AuNPs was PAS but not electroless plating, electroless plating of Au layers was conducted on graphene. The graphene sheet was

#180639 - $15.00 USD Received 27 Nov 2012; revised 16 Feb 2013; accepted 17 Feb 2013; published 8 Mar 2013

immersed into $AuCl_4^-$ electrolyte without laser irradiation. After immersion for certain periods, the graphene sample was removed from the electrolyte for AFM measurement in ambience. Figure 4(a) shows the AFM images of the pristine graphene and the morphological evolution of the electroless-plated Au layer on graphene after 40 s, 80 s, and 10 min of immersion. Before immersion, the graphene was a single layer with a clean surface. After 40 s, a trace of Au seeds was observed on the surface of graphene. The coverage of Au on graphene increased with the immersion time until the Au was grown laterally into a continuous layer, which covered the entire surface of graphene, as shown in the displayed image taken after 10 min immersion. Figure 4(b) shows the height profiles near the graphene edge before and after immersion. Au seeds ceased growing vertically when their height reached 2 nm, indicating that the growth was a self-limited process.

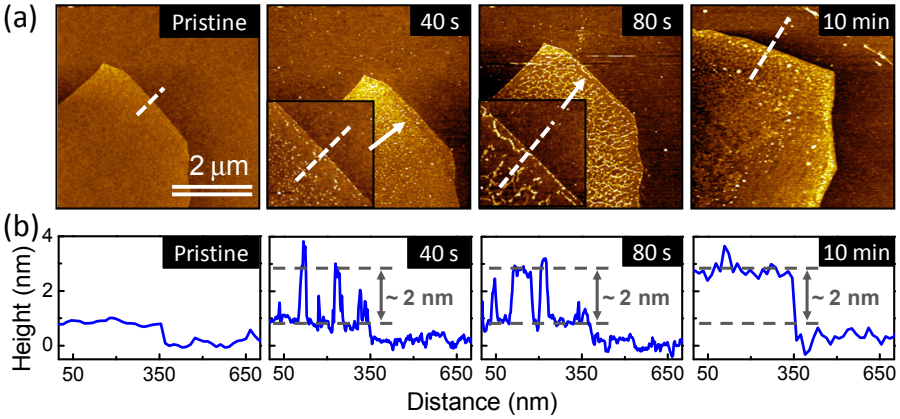

Fig. 4. (a) Morphologic evolution of plated Au on graphene with the immersion duration in $AuCl_4^-$ electrolyte. The insets in (a) is to illustrate the details of plated Au of 40 s and 80 s immersion. (b) The corresponding cross-sectional profiles along the dash lines in (a).

The chemical composition of the electroless-plated Au layer was characterized by μ-PES with a photon energy of 380 eV. The SiO_2/Si substrate was coated with a transparent conductive indium tin oxide thin layer to avoid charging effect during measurement. A bi-layer graphene (BLG) sheet was prepared on the substrate. The BLG was then subjected to electroless plating for 10 min. In Fig. 5(a), the spectrum shows metallic Au photoelectron peaks of $4f_{7/2}$ and $4f_{5/2}$ at 84.0 eV and 87.6 eV, respectively, which indicated the existence of Au thin layer. The signal was weak because of the slim amount of Au. Figure 5(b) shows the C 1*s* spectra of pristine graphene and Au-plated graphene. The C 1s spectra were deconvoluted into carbon sp^2 and sp^3 peaks. The binding energy of the sp^2 peak of the Au-covered graphene (284.25 eV) was approximately 0.11 eV lower than that of the pristine graphene (284.36 eV). The decrease of binding energy of the Au-plated graphene was attributed to the lowering of its Fermi energy, resulting from the charge transferring from graphene to Au [17]. The higher sp^3 peak intensity of pristine graphene could be attributed to damage from the longer exposure to the synchrotron X-ray, because the pristine graphene had a low visibility in the SPEM system, and thus, it took longer to be observed for μ-PES measurement.

The formation of Au can be expressed by the reduction of $AuCl_4^-$ on the graphene:

$$AuCl_4^- + 3e^- \rightarrow Au^0 \downarrow + 4Cl^- . \quad (3)$$

The reduction of $AuCl_4^-$ is spontaneous because the reduction potential of the electrolyte is 1.0 V, which is higher than that of graphene (0.22 V) [10,11]. Here, the graphene was a reductant, giving electrons to $AuCl_4^-$. During the reduction of Au, electrons transferred from graphene to electrolyte, resulting in the increase of the work function of graphene, as well as

#180639 - $15.00 USD Received 27 Nov 2012; revised 16 Feb 2013; accepted 17 Feb 2013; published 8 Mar 2013

reduction potential of graphene. The reaction stopped automatically as the reduction potential of graphene met that of electrolyte. Except for the 2 nm plated Au thin layer on graphene, no AuNP was observed on the surface of graphene. Hence, the formation mechanism of AuNPs was the PAS rather than electroless plating. Note that, during the growth of AuNPs on graphene by PAS, the 2 nm thick Au layer was also deposited by electroless plating. No Au seed was formed on the insulated SiO_2. We suggest that PAS of AuNPs on graphene was a seed-mediated process [18]. To apply PAS of AuNPs on typical optical components, one has to prepare graphene on the components first.

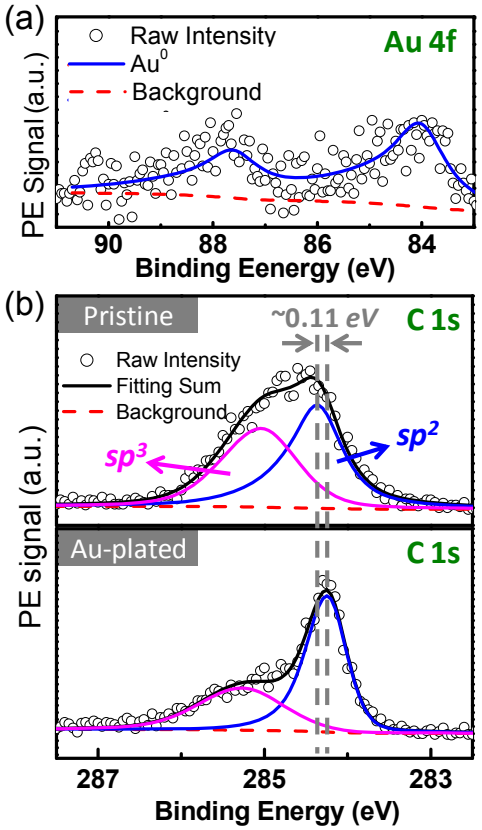

Fig. 5. (a) Au 4f core-level photoelectron (PE) spectrum taken from Au-plated BLG, and (b) C 1s core-level spectra of pristine BLG and Au-plated BLG.

To observe the Raman enhancement with the increase of the size of the synthesized AuNPs, the Raman spectra of graphene were taken *in situ* during PAS. Figure 6(a) shows the Raman intensities of the G-band and 2D-band with growth time *t*. Both G-band and 2D-band Raman intensities began to increase after 1 min, which was nearly coincidental with the time that AuNPs grew on graphene. Therefore, the Raman signals were considered to have been enhanced by the LSP of AuNPs. Figure 6(b) shows the *ex situ* Raman spectra of the pristine graphene and graphene with a single 100 nm AuNP (in ambience). A remarkable D-band signal was observed for the graphene with synthesized AuNPs but no D-band was detected with the pristine graphene. The D-band signal was attributed to the lattice deformation caused by the local intensive plasmonic EM field of AuNPs (see the results of 3D FDTD calculation shown in below). Compared with the Raman spectrum of pristine graphene, the G-band and 2D-band Raman peaks of graphene with an AuNP exhibited a considerable enhancement by 40 and 16 times, respectively. The area covered by a 100 nm AuNP was only approximately 1/25 of the area irradiated by the 500 nm spot. Thus, the effective enhancement of the G-band

#180639 - $15.00 USD Received 27 Nov 2012; revised 16 Feb 2013; accepted 17 Feb 2013; published 8 Mar 2013

caused by LSP could be as high as 10^3 times. The enhancement was suppressed in solution because of the damping effect of the solution on LSP and light scattering at the air/solution interface. In addition, no enhancement was observed to the Raman signals of graphene with the 2 nm electroless-plated Au layer, suggesting that the thin Au layer may not contribute to the Raman enhancement of graphene with AuNPs.

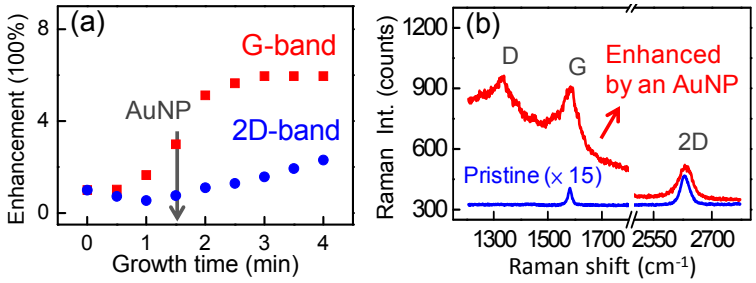

Fig. 6. (a) Enhancement of G-band and 2D-band Raman intensity taken *in situ* during PAS. The arrow indicated when synthesized AuNPs were deposited on graphene. (b) *Ex situ* Raman spectra taken on pristine graphene and graphene with 100 nm AuNP in ambience.

To model the plasmonic EM field by 3D FDTD simulation, a single AuNP placed on a 2 nm thick Au film (in air), a layer of 1 nm thick graphene, and an infinite SiO_2 substrate were considered, as shown in Fig. 7(a). The substrate lay on the X-Y plane. The incident EM field with X-polarization propagated along the −Z direction. In the calculations, the total-field scattered-field source was applied. Figure 7(b) exhibits the simulated electrical field distributions along the X-Z plane and X-Y plane with the AuNP size of 25 and 100 nm, respectively.

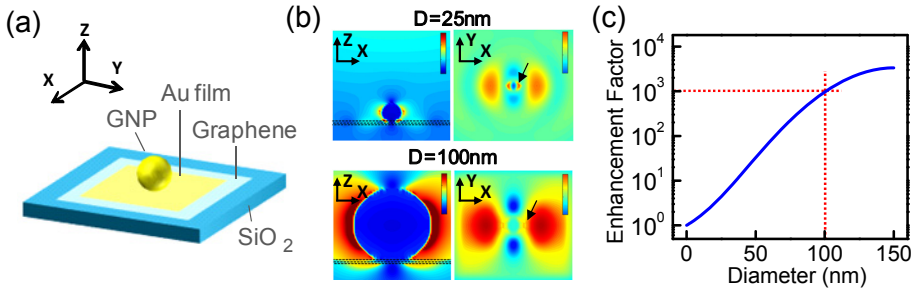

Fig. 7. (a) Illustration of a synthesized AuNP and a plated Au layer on graphene for modeling of EM field by 3D FDTD simulation. (b) Representative resultant absolute electric field distributions of 150 nm × 150 nm along the X-Z plane (across the center of AuNP) and X-Y plane (at the upper surface of graphene), respectively. The dashed lines denote where the graphene and plated Au layer locate, and the arrows indicate where the hot spots are. In the color scale, "blue" presents the zero field intensity and "red" the maximum field intensity. (c) The enhancement factor at the upper surface of graphene with respect to the diameter of AuNPs, where the dotted lines indicate the *EF* with a 100 nm AuNP is approximately 10^3.

The strong field intensity appears in the vicinity of the AuNP surface because the LSP. The field were coupled into the Au layer and graphene sheet. There was an additional strong field was observed at the gap between the AuNP and Au layer near the bottom of the AuNP, which was attributed to the hot spot effect. The resultant field intensified with the increase of particle size and the coupled field became dominant for the 100 nm AuNP at the graphene surface. To calculate the field enhancement by LSP, the field intensity was integrated over a circular area of laser spot size at the upper surface of the graphene with and without the existence of an AuNP. The enhancement factor (*EF*) of SERS can be obtained from the expression $|I_{NP}|/|I_0|$, where I_{NP} and I_0 are respectively the integrated power with and without an

#180639 - $15.00 USD Received 27 Nov 2012; revised 16 Feb 2013; accepted 17 Feb 2013; published 8 Mar 2013

AuNP [19]. Figure 7(c) shows the relationship between the particle size and *EF*. The *EF* increased largely with respect to the particle size. The calculated *EF* with a 100 nm AuNP is consistent with the effective enhancement of the G-band Raman signal in Fig. 6(b), indicating the Raman signals were enhanced by LSP. Accordingly, the D-band Raman signal of graphene along with AuNPs is suggested to be attributed to the lattice deformation caused by the local intensive plasmonic EM field induced by the synthesized AuNPs.

The SERS of AuNP-loaded graphene can be applied to stress sensors, because the Raman G peak shifts with the uniaxial strain in graphene by a shift rate of $-5\omega_0^{-1}$ ($cm^{-1}MPa^{-1}$), where ω_0 is the G peak position at zero stress for graphene [20]. The speed of stress sensing will be improved due to the enhancement of Raman signals of graphene. Furthermore, PAS can produce the SERS active substrates for ultrasensitive detections of microbes [21], cellular components [22], and biomolecules [23].

4. Conclusion

The preparation of AuNPs on graphene by PAS has been demonstrated in the $AuCl_4^-$ electrolyte. Because PAS of AuNPs requires only the $AuCl_4^-$ electrolyte and has a steady volume growth rate of AuNPs, it is a convenient and reliable method for producing AuNPs on graphene. AuNPs can be grown on selective areas and the distribution of AuNPs can be controlled by focusing the laser. In addition to AuNPs by PAS, a 2 nm thick Au thin layer was simultaneously formed on graphene by electroless plating. SERS of graphene was observed, and the Raman enhancement by a single 100 nm AuNP was 10^3 times. The 3D FDTD calculation indicates that the enhancement is attributed to the LSPs of AuNPs.

Acknowledgments

This work was supported by National Science Council, Taiwan and the Project of Global Research & Education on Environment and Society, Tunghai University.

#180639 - $15.00 USD Received 27 Nov 2012; revised 16 Feb 2013; accepted 17 Feb 2013; published 8 Mar 2013